ELSEVIER

Biochimica et Biophysica Acta 1569 (2002) 86–104

BIOCHIMICA ET BIOPHYSICA ACTA
BBA

www.bba-direct.com

Spatiotemporal dynamics of contact activation factors of blood coagulation

Andrei Yu. Kondratovich *, Alexandra V. Pokhilko, Fazoil I. Ataullakhanov

Research Center for Hematology, Russian Academy of Medical Sciences, Novozykovskii proezd 4a, Moscow 125167, Russia

Received 15 May 2001; received in revised form 12 November 2001; accepted 20 November 2001

Abstract

A new in vitro model is proposed for studying the spatiotemporal distributions of activated clotting factors, in which clotting is activated in a thin layer of nonstirred plasma supplemented with a fluorogenic substrate and is monitored by fluorescence from its cleavage product. Analysis of the spatiotemporal dynamics of factor XIa and kallikrein in glass-activated human plasma provides evidence that both contact factors remain restricted to the glass surface and possibly a narrow boundary zone (<0.1 mm). The kinetics of factor XIa and kallikrein studied by a new method (in nonstirred plasma) coincided with those studied fluorimetrically with full stirring: their concentrations rapidly rose for the first few minutes after activation and then slowly declined. Factor XI and prekallikrein activation is likely to be restricted by the limited number of sites available for binding to the surface. The maximum concentration of the active factors was estimated at 2×10^8 molecules per mm^2 at the glass surface (irrespective of stirring). At the plastic surface, this value was 15–30 times lower.

Keywords: Contact activation system; Blood coagulation; Spatiotemporal dynamics; Factor XIa; Kallikrein; Citrated plasma

1. Introduction

An important role in hemostasis is played by its plasma component, that is, the coagulation system [1]. Vessel wall damage initiates the cascade of biochemical reactions in plasma resulting in the formation of an insoluble fibrin clot. The nascent clot must grow fast to seal the damaged area of the vessel wall while leaving the lumen patient. In other words, clot formation must proceed fast and be localized to the site of injury. What are the factors that control the spatiotemporal dynamics of clot formation and determine its size? Conceivably, these questions may be answered by observing how a clot evolves and grows in a thin layer of nonstirred human plasma in vitro. The first qualitative results describing the dynamics of thrombin and fibrin formation on a glass surface in such a system were reported by Ataullakhanov et al. [2]. Compact fibrin clots were formed around foci of activation. The clot thickness was invariably about 1 mm, whatever the size and shape of the glass activator. Moreover, clots grew to the same size in platelet-free plasma (PFP), platelet-poor plasma (PPP), platelet-rich plasma (PRP), and whole blood [2], suggesting that the spatiotemporal dynamics of clot growth observed in vitro was determined by the plasma (rather than cellular) component of hemostasis.

The surface of glass activates the intrinsic pathway of coagulation [3]. Its first stage is the so-called contact activation, which includes factors XII, XI, kallikrein, and high molecular weight kininogen (HMWK) [3]. The latter acts as a cofactor. The process starts with factor XII binding to the glass surface. Upon binding, it is converted into factor XIIa, which autocatalytically enhances its own production and catalyzes the reactions giving rise to kallikrein and factor XIa [4]. Kallikrein, in its turn, activates HMWK, significantly accelerating factor XIIa and thereby factor XIa formation [5]. Following the appearance of factor XIa, factors IXa, Xa, thrombin, and fibrin are sequentially generated [1]. Fibrin monomers polymerize to form a clot. In this way, factor XIa produced in the contact phase of coagulation sets the initial conditions for the subsequent process of fibrin formation. Therefore, the dynamics of clot growth and the final clot shape may significantly de-

Abbreviations: PFP, platelet-free plasma; PPP, platelet-poor plasma; PRP, platelet-rich plasma; AMC, 4-methyl-7-aminocoumarin; LBTI, lima bean trypsin inhibitor; SBTI, soybean trypsin inhibitor; HMWK, high molecular weight kininogen; α_2MG, α_2-macroglobulin; kall–α_2MG, kallikrein–α_2-macroglobulin complex

* Corresponding author. Fax: +7-095-212-5531.
E-mail address: ak@blood.ru (A.Y. Kondratovich).

0304-4165/02/$ – see front matter
PII: S0304-4165(01)00247-1

pend on the spatial distribution of contact activation factors XIa and kallikrein.

We are not aware of any data in the literature concerning the spatial distribution of these factors. However, there are a few studies in which the ratios between the surface-bound and free forms of factor XIa and kallikrein have been determined using ^{125}I-labeled precursors in the system with full stirring [5,6]. In dilute kaolin-activated human plasma, factor XIa was formed only on the activating surface and barely dissociated into the bulk [6]; the free to surface-bound factor XIa ratio was estimated at 1:10 [5]. Prekallikrein could be activated not only on the surface, but also in solution. The kallikrein formed on the surface easily dissociated into the bulk [6], resulting in the free to surface-bound kallikrein ratio of 5:1 [5]. However, with the method used in that study, it was impossible to judge whether the kallikrein remained free in solution or was inactivated by plasma inhibitors. The spatial distribution of factor XIa and kallikrein in undiluted plasma also remains an open question. More recent studies of the intrinsic pathway in a capillary flow reactor [7] have shown that, at low flow rates (wall shear rate 40 s^{-1}), considerable amounts of free factor XIa are produced in undiluted plasma over the first 2–3 min of its activation with glass and rapidly disappear thereafter. Although surface-bound factor XIa was not measured, indirect evidence suggested that its concentration did not change for at least 30 min, remaining at a much greater level than that of free factor XIa observed immediately after activation.

The kinetics of changes in contact activation factors, even in systems with full stirring, is not known in sufficient detail. Numerous studies describe systems reconstructed from purified proteins [4], but the kinetics of whole plasma activation has been investigated only with high concentrations of kaolin [8], and only the total amidolytic activity of plasma has been measured. The contributions of individual enzymes (factor XIa, kallikrein) to the total activity have been assessed by inhibitor analysis in fully activated inhibitor-depleted plasma [9,10]. Therefore, this study was designed to examine in more detail the kinetics of factor XIa and kallikrein formation in moderately activated plasma and to visualize how the activated factors spread from the activating surface into the bulk.

Specifically, we studied the dynamics of generation of contact activation factors and their spatial distribution in nonstirred plasma brought in contact with glass. The data obtained agree well with the data on the kinetics of these factors in systems with full stirring. Factor XI and prekallikrein became activated in 1.5–3 min. In the subsequent 20–30 min, their amidolytic activity towards fluorogenic substrates decreased approx. 2-fold and remained constant for about 0.5 h thereafter. Over 2 h of observation, both factor XIa and kallikrein remained restricted to the activator surface, not spreading or spreading away by no more than 0.1 mm.

2. Materials and methods

2.1. Materials

Healthy donor blood was collected in a citrate–phosphate–dextrose solution-containing polyvinyl chloride blood bag with one integrally attached satellite bag (Baxter) and centrifuged at $2400 \times g$ for 20 min at 22°C. The supernatant PPP was transferred to the satellite container under closed-system conditions and stored sterile in this container at room temperature for no more than 3 days before the experiment. A sterile technique was used to sample plasma during experiments.

Plasma deficient in α_2-macroglobulin was prepared by incubating PPP with 40 mM methylamine for 2 h at room temperature [11]. The distributions of factor XIa, kallikrein, and thrombin were studied using fluorogenic substrates referred to below as S, S_k and S_2, respectively. Substrate S (L-pyroglutamyl-prolyl-arginyl-7-amino-4-methylcoumarin ·HCl, a fluorogenic analogue of S_{2366}), which is efficiently cleaved by both factor XIa and kallikrein [12], and substrate S_2 specific for thrombin (*t*-*N*-butoxycarbonyl-alanyl-prolyl-arginyl-7-amino-4-methylcoumarin) [13] were synthesized by Dr. V.F. Pozdnev (Institute of Biological and Medical Chemistry, Russian Academy of Medical Sciences, Moscow, Russia). Substrate S_k (*N*-carbobenzyloxy-phenylalanine-arginyl-7-amino-4-methylcoumarin) for kallikrein was from Sigma. A product of substrate cleavage 4-methyl-7-aminocoumarin (AMC) fluoresces in the blue range of the spectrum, with the emission maximum at $\lambda_{em} = 440$ nm and the excitation maximum at $\lambda_{ex} = 380$ nm. The diffusion coefficient for AMC was assessed in experiments with plasma containing 0.2% low melting point agarose (Fluka, Germany).

To record the individual contributions of contact activation factors, lima bean trypsin inhibitor (LBTI; Sigma) and soybean trypsin inhibitor (SBTI; Sigma) were used. SBTI is known to immediately and completely inhibit factor XIa and kallikrein at a concentration of 200 μg/ml SBTI [12]. LBTI was used at a concentration of 250 μg/ml at which it immediately and completely inhibits factor XIa but has no effect on kallikrein [12].

2.2. Experiments in homogeneous systems

2.2.1. Sample processing

Standard polystyrene cuvettes measuring $10 \times 10 \times 40$ mm (Brand) were used in experiments with full stirring. Their walls were shown to cause only a weak contact activation of the plasma. Cuvettes were filled with plasma directly from bag tubing, avoiding contact with any additional surfaces. A JY 3A fluorescence spectrophotometer (Jobin Ivon, France) was used to record AMC fluorescence ($\lambda_{em} = 440$ nm; $\lambda_{ex} = 380$ nm). The AMC concentration was determined from a calibration curve constructed

for each experiment using plasma dilutions of a known amount of AMC.

Each PPP sample was supplemented with substrate S or S_k and stirred at 37°C for 20 min prior to measurements. The final substrate concentration was varied. All additions to a plasma sample were made in 0.15 M Tris–HCl buffer (pH 7.4 at 37°C) containing 0.1 M NaCl and accounted for 16% of its final volume (1.8 ml). To contact activate the plasma preincubated with the fluorogenic substrate, 100 mg of 1 mm dry glass beads per sample was quickly added. The total glass surface area to plasma volume ratio was estimated at 0.12 $mm^2/\mu l$. The kinetics of AMC accumulation was recorded for various intervals of time. If the long-term kinetics (10 min or more) was studied, the substrate was added 7 min before measurements to avoid substrate depletion. A comparison of the kinetic curves for substrate S or S_k cleavage recorded on 3 consecutive days of room temperature plasma storage revealed no significant changes between them (data not shown). Therefore, all experiments were performed during the first 3 days of plasma storage.

2.2.2. Substrate S and S_k cleavage by plasma in polystyrene cuvettes

The rate of substrate cleavage during a 20 min incubation at 37°C before addition of glass beads was referred to as the background rate. It was small with substrate S_k, no more than 10% of the rate in the presence of glass beads. With substrate S, the background cleavage rate was greater (about 35% of the rate in the presence of the activator). Therefore, to properly assess the activating effect of glass, we studied the dependence of the background cleavage rate (that is, the amidolytic activity of plasma placed in a polystyrene cuvette) on the substrate S concentration (Fig. 1). This dependence was well approximated by the Michaelis–Menten equation, with the Michaelis constant K_m being about 300 μM. The background amidolytic activity of plasma could not be suppressed by addition of 200 μg/ml SBTI, suggesting that neither factor XIa, nor kallikrein accounted for the background enzymatic activity of plasma toward substrate S. The background rate was subtracted from all the kinetic curves presented below.

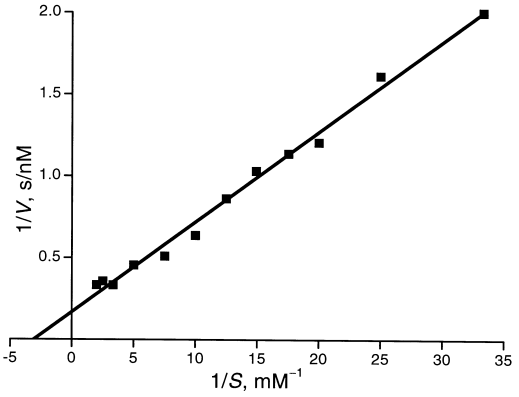

Fig. 1. Lineweaver–Burk plot for amidolytic activity (V, nM/s) of plasma induced by its contact with polystyrene cuvette walls against substrate S (37°C, continuous stirring). The reaction mixture consisted of 1510 μl of plasma and 290 μl of 0.15 M Tris–HCl buffer (pH 7.4 at 37°C) containing 0.1 M NaCl and substrate S at various concentrations. Before recordings, the samples were stirred for 20 min at 37°C.

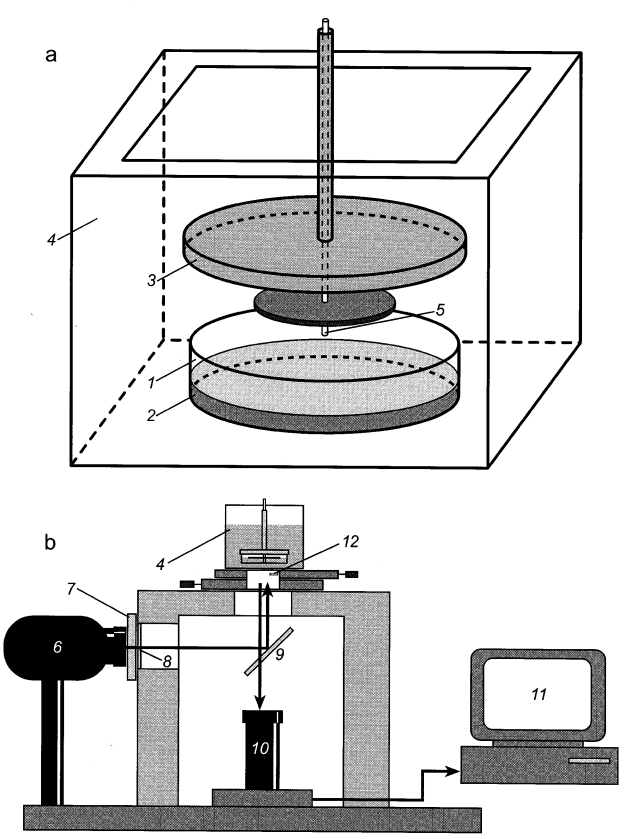

Fig. 2. Scheme of (a) temperature-controlled measurement compartment with a Petri dish and (b) the experimental setup for excitation of fluorescence and recording its spatiotemporal distributions. 1, polystyrene Petri dish; 2, substrate S-supplemented plasma aliquot; 3, dish's opaque lid; 4, water jacket; 5, tip of a glass capillary (activator of coagulation); 6, mercury lamp; 7, aqueous heat-blocking filter; 8, glass filter; 9, semitransparent mirror; 10, CCD camera; 11, computer; 12, fluorescing plastic label. See text for description.

A similar background activity toward other substrates was described previously [8]. It is conceivable that its source is the kallikrein–α_2-macroglobulin (kall–α_2MG) complex, which is inactive in cleaving coagulation factors but retains the activity against low molecular weight substrates [14]. In fact, the background amidolytic activity was several times lower in α_2-macroglobulin-deficient plasma than in normal plasma (data not shown).

2.3. Experiments in nonstirred plasma

2.3.1. Sample processing

The formation of activated factors induced by contact with a glass surface was studied for the two-dimensional case, that is, in a thin layer of nonstirred plasma. Under such conditions, plasma loses CO_2, and its pH rapidly

increases. Therefore, 10% lactic acid was added to plasma at 37°C for 1.5 h before the experiment. We varied the acid volume from 10 to 25 μl per ml plasma to determine how much acid had to be added to bring the pH of that particular plasma to 7.2–7.4 by the end of a 1.5 h incubation. After this treatment, the plasma pH remained unchanged throughout the experiment [15].

A polystyrene Petri dish 35 mm in diameter (Fig. 2_1), which is only a weak activator by itself, was filled with a 2 ml aliquot of pH-stabilized plasma supplemented with 500 μM substrate S (Fig. 2_2). All additions were made in 0.15 M Tris–HCl buffer (pH 7.4 at 37°C) containing 0.1 M NaCl and accounted for 16% of the final volume of the plasma sample. The dish was tightly sealed with an opaque lid (Fig. 2_3), which had a hole at its center with an activator passed through it. The activator was a dry glass capillary 1.3 mm in diameter with the lower end hermetically sealed (Fig. 2_5). A polystyrene disk was set tightly on this capillary 2 mm from its lower end at a right angle to the axis. When assembled, the activator was positioned so that its lower end could not touch the plasma surface, and the disk was beneath the lid. The sealed dish was transferred to a water jacket (Fig. 2_4) maintained at 37°C. After equilibrating the sample at 37°C for 5 min, we quickly let the activator down until its end touched the bottom. The plasma formed a horizontal layer 2 mm thick between the bottom of the dish and the polystyrene disk. At the center of this layer, there was a glass activator (capillary walls below the disk; Fig. 2_5). The area of the glass surface in contact with plasma was 8.2 mm^2.

2.3.2. Recording the spatiotemporal dynamics of fluorescence

The coagulation factors activated by contact with glass cleave substrate S, giving rise to AMC. Its fluorescence was recorded using a specially constructed laboratory setup (Fig. 2b). The plasma sample in a water-jacketed Petri dish (Fig. $2b_4$) was illuminated from below with excitation light reflected off a semitransparent mirror (Fig. $2b_9$). The light source was a 250 W DRSh-250 mercury lamp (Fig. $2b_6$). An aqueous heat-blocking filter (Fig. $2b_7$) and a UFS-6 UV filter (Fig. $2b_8$) that blocked the visible portion of the lamp spectrum were placed in the excitation path. The AMC fluorescence was recorded with a CCD camera (Electrium, USA; Fig. $2b_{10}$) mounted behind the semitransparent mirror. The recorded field of view measured 9.0×6.5 mm. The blue channel of the RGB output signal of the CCD camera spanned the entire range of AMC fluorescence. The image data were continuously transferred to a computer (Fig. $2b_{11}$), displayed on its monitor, and saved at specified intervals. A piece of fluorescing plastic (Fig. $2b_{12}$) was fixed just beneath the water jacket so that its image was always in the field of view of the camera. During data processing, it served as a label whose fluorescent properties did not vary over time.

The setup was tested for linearity and found to be linear up to 80 μM AMC. No convection-related distortions were detected. A software package for data processing that was tailored to this setup made it possible to correct for the nonuniform illumination of the field of view and for the instability of the mercury lamp. In the corrected data, the nonuniformity of illumination across the field was less than 5%, its temporal instability was less than 15%, and the spatial resolution was 10 μm. To correct the raw image for the nonuniform illumination and to determine the AMC concentration, we used a calibrating image of a sample of the same plasma to which AMC was added to a known final concentration (see Appendix A). When analyzing the images, we arbitrarily drew a scan line from the activator's center. This procedure allowed us to go over to a set of one-dimensional profiles of the fluorescence intensity for all frames of the experiment, including the calibrating image. Using the latter, we obtained this set in the normalized form, that is, we obtained a time series of spatial AMC distributions for each experiment (see Appendix A). The only serious distortion that remained after implementing this procedure was an unduly smoothed AMC distribution over a 30–50 μm interval adjacent to the activator surface. Therefore, only rough estimates could be obtained for this region of interest.

2.3.3. Deriving the spatial distribution of activated factors from the distribution of AMC, a fluorescing product of substrate cleavage

With the setup described above, a series of the spatial AMC distributions could be obtained that corresponded to various moments of time after bringing the plasma in contact with glass. Knowing AMC(x,t) is yet insufficient to immediately derive the spatial distribution of activated factors for various moments of time (that is, factor activities as functions of time and coordinate $F(x,t)$), because free AMC after being cleaved from the substrate by activated factors diffuses in plasma away from the site of cleavage. To derive $F(x,t)$ from AMC(x,t), we have developed a special computer program based on the following assumptions: (i) once AMC has appeared, it freely diffuses in plasma; (ii) the substrate from which AMC is cleaved also freely diffuses; as the substrate is hydrolyzed, its concentration decreases; and (iii) the rates of AMC generation and substrate cleavage are equal and follow the Michaelis equation.

The system under study is centrally symmetrical; therefore, its scanning strictly along a radius converts the two-dimensional problem into a quasi-one-dimensional problem. For segment $[X_b,X_f]$, with X_b corresponding to the activator boundary and X_f to the boundary of the field of view, the following set of equations can be written:

$$\frac{\partial \mathrm{AMC}(x,t)}{\partial t} = \frac{D_{\mathrm{AMC}}}{x}\frac{\partial}{\partial x}\left(x\frac{\partial \mathrm{AMC}(x,t)}{\partial x}\right) + V_{\mathrm{AMC}}(x,t) \quad (1)$$

$$\frac{\partial S(x,t)}{\partial t} = \frac{D_S}{x}\frac{\partial}{\partial x}\left(x\frac{\partial S(x,t)}{\partial x}\right) - V_{AMC}(x,t) \quad (2)$$

$$V_{AMC}(x,t) = \frac{k_2 S(x,t) F(x,t)}{K_m + S(x,t)} \quad (3)$$

where $V_{AMC}(x,t)$ denotes the rate of AMC generation; $S(x,t)$ and $F(x,t)$ stand for the substrate and enzyme concentration, respectively; D_{AMC} and D_S are the diffusion coefficients for AMC and the substrate, respectively; and k_2 and K_m are the kinetic constants for enzymatic cleavage of substrate S. Eq. 1 for AMC contains terms corresponding to its enzymatic production and subsequent diffusion. Eq. 2 describes the enzymatic degradation of the substrate and its diffusion. Eq. 3 describes the Michaelis–Menten kinetics of enzymatic AMC production.

From the recorded AMC(x,t), we could quantitatively determine the derivatives $\partial AMC(x,t)/\partial t$ and $\partial/\partial x(x(\partial AMC(x,t)/\partial x))$. Substituting them into Eq. 1, we obtained $V_{AMC}(x,t)$. Knowing $V_{AMC}(x,t)$ and solving Eq. 2 by the sweep method [16], we found $S(x,t)$, setting the initial and boundary conditions in the form: $S(x,0) = S_0$, $\partial S(X_b,t)/\partial t = 0$ (impermeable glass surface at the left boundary), and $S(X_f,t) = S_0$. The latter corresponds to the assumption that, over the time of experiment, the substrate concentration was maintained at S_0 at the right boundary, because no activated factors reached it even by the end of the experiment and because the substrate was present in considerable amounts in the Petri dish beyond the field of view. With the known $V_{AMC}(x,t)$ and $S(x,t)$, the distribution $F(x,t)$ could be found from Eq. 3.

The algorithm described holds when only one enzyme cleaves the substrate. However, it is not the case for substrate S, which, as shown below, is hydrolyzed by at least three proteins: factor XIa, kallikrein, and presumably the kall–α_2MG complex. The Michaelis scheme can be used to describe their total amidolytic activity toward substrate S (see Fig. 9c). Eqs. 1 and 2 hold in this case; Eq. 3 also retains its form if the constants k_2 and K_m are replaced with the apparent constants k_{2app} and K_{mapp} for the substrate cleavage by collectively factor XIa, kallikrein, and the kall–α_2MG complex, and $F(x,t)$ is considered to be a function of the concentration of these three proteins. Knowing this function, we cannot judge how the individual factors are distributed over the range where $F(x,t)$ differs from zero, but we are confident that none of them extends beyond the boundaries of this range. The apparent Michaelis constant K_{mapp} for substrate S was estimated at 300 μM (see Fig. 9c). The constant k_{2app} is a multiplier of $F(x,t)$ in Eq. 3 and affects only the absolute value of the product but not the $F(x,t)$ profile. As a first approximation, we set k_{2app} to 300 s^{-1}, the value reported for hydrolysis of substrate S_{2366} (a chromogenic analogue of substrate S, with *p*-nitroaniline instead of AMC) by factor XIa [12].

2.3.4. *Experimental validation of the algorithm and the program for deriving the spatial distribution of activated factors*

To derive the spatial distribution of activated factors

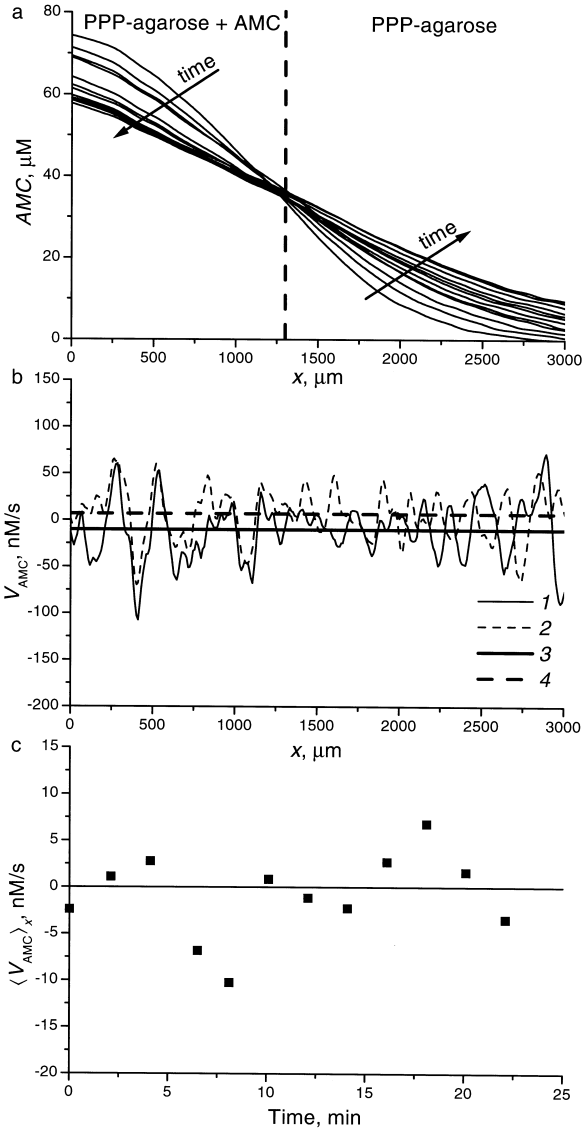

Fig. 3. (a) Diffusion-driven AMC redistribution in a system wherein 0.2% agarose gel prepared in PPP (on the right) borders (dashed line) on the same gel prepared in PPP containing 80 μM AMC (on the left). (b) Derivation of the source function V_{AMC} from the profiles shown in panel a. (c) V_{AMC} averaged over x($\langle V_{AMC} \rangle_x$) calculated from the data in panel b plotted versus time. (a) Determination of the diffusion coefficient of AMC. The first curve was recorded 3 min after the start of the experiment and the subsequent curves at 2 min intervals. According to [17], $\partial AMC(x)/\partial x$ is the Gaussian function in this case, with $\sigma^2 = 2D_{AMC}t$, where t is the time from the start of diffusion. Hence, $D_{AMC} = (7.9 \pm 0.5) \times 10^{-6}$ cm^2/s. (b) An example of zero signal processing. The source function V_{AMC} was calculated from the data presented in panel a (only AMC redistribution and no production) using the algorithm that we developed. Shown are profiles 1 and 2 only (8 and 18 min from the start of the experiment), because their mean values (3 and 4, respectively) differ from zero most significantly, being, however, two orders of magnitude smaller than those observed in glass-activated plasma (data not shown).

using the program developed, one has to know the exact value of the diffusion coefficient for AMC (D_{AMC}) in plasma. We determined D_{AMC} experimentally with a technique making it possible to avoid convective mixing of AMC. A Petri dish was filled with 0.2% agarose prepared in PPP to give a layer 2 mm thick. After gelation of the mixture, it was removed from the left half of the dish, which was then filled to the same height with 0.2% agarose prepared in PPP containing 80 μM AMC. The boundary between the gels was flat. AMC diffused from the left half of the dish to its right half (Fig. 3a). According to [17], the derivatives of the AMC distributions with respect to coordinate are described by the Gauss function, with $\sigma^2 = 2D_{AMC}t$, where t is the time from the start of diffusion. Analysis of the distributions presented in Fig. 3a leads to an estimate of $(7.9 \pm 0.5) \times 10^{-6}$ cm^2/s for D_{AMC} in the agarose-containing plasma. As agarose was added to a low concentration, D_{AMC} in plasma is likely to be within the same limits. Using the data reported in [18], the diffusion coefficient of substrate S in plasma was estimated at 4.4×10^{-6} cm^2/s from its molecular mass of 600 Da.

The method developed for deriving the activated factor distributions was validated in experiments with the known shape of the distribution. First, we used it to process the data of an experiment designed to determine the diffusion coefficient of AMC (Fig. 3). In this and other cases when the experimental system was symmetrical with respect to plane, rather than being centrally symmetrical, the gradient in diffusion Eqs. 1 and 2 was written as $D_{AMC}(\partial^2 AMC(x,t)/\partial x^2)$ and $D_S(\partial^2 S(x,t)/\partial x^2)$ respectively.

In this experiment, no source of AMC existed; only its initially nonuniform distribution rapidly progressed to a uniform one. The source function V_{AMC} calculated for this experiment with the algorithm developed represents a family of noisy curves (Fig. 3b) in which no regular pattern could be detected. Averaging each of these curves over space (Fig. 3c), we found that the AMC production rate fluctuated around zero. This is an expected result, as the dish contained no sources that produced AMC.

In the second experiment performed to validate the data processing algorithm, we added 200 μM substrate S_2 ($k_2 = 130$ s^{-1}, $K_m = 13$ μM [13]) to a Petri dish with 73 pM thrombin in a Tris–HCl buffer. In this way, we obtained a spatially uniform distribution of the enzyme. The AMC concentration was isotropic and grew rapidly (Fig. 4a). The thrombin distribution reconstructed using our algorithm was a set of noisy curves (Fig. 4b, curves 1–3). Being approximated with a linear function, these curves became a set of straight lines (Fig. 4b, curves 4–6), which were almost parallel to the abscissa. These data demonstrated that the program introduced no systematic biases into the spatial distribution to be determined. The mean thrombin concentration calculated from these data (Fig. 4c$_1$) only weakly fluctuated over time, with the amplitude of fluctuations being less than 15% (Fig. 4c). The level of spatial noise did not exceed 25% (Fig. 4b, curves 1–3). The mean thrombin concentration of 79 ± 12 pM calculated with the program developed (Fig. 4c$_2$) is in close agreement with the thrombin concentration that was added to the dish (73 pM, Fig. 4c$_3$).

The algorithm for reconstructing the spatiotemporal distributions of activated factors from fluorescence images plays a decisive role in our data-processing system. The data described above show that the algorithm is robust in

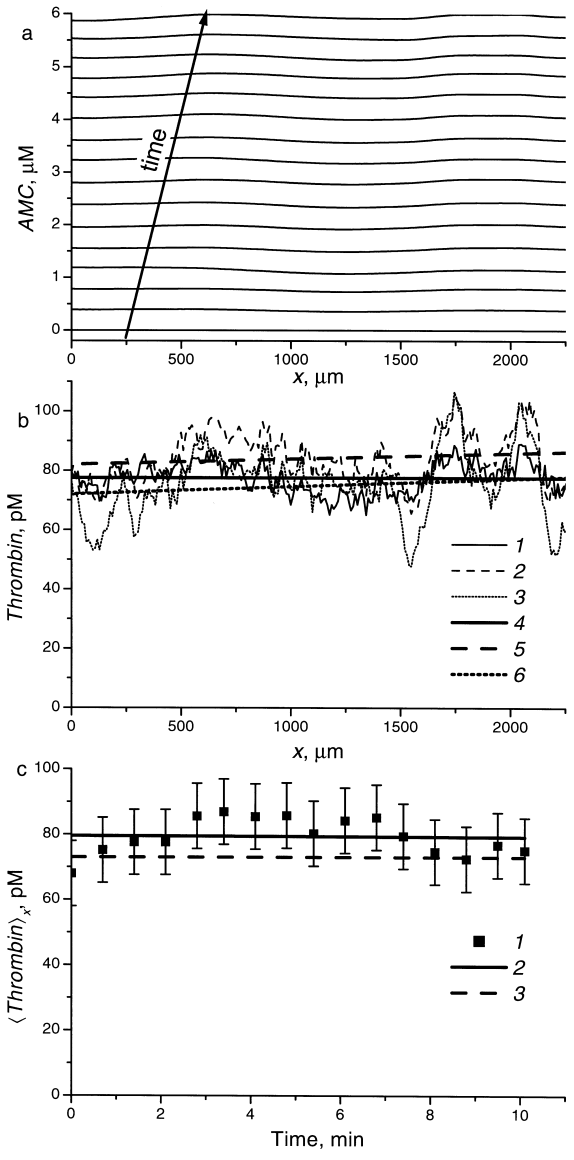

Fig. 4. Algorithm validation in constant source experiments (thrombin solution). (a) AMC profiles recorded at 40 s intervals in a Petri dish containing 73 pM thrombin in a 0.15 M Tris–HCl buffer (2 ml) to which 200 μM substrate S_2 was added at time 0. (b) 1–3, thrombin distributions reconstructed at 4 min intervals from the AMC(x,t) data in panel a; 4–6, their linear approximations. (c) 1, mean thrombin concentration determined by averaging the reconstructed thrombin distribution over space ($\langle Thrombin \rangle_x$) plotted versus time; 2, its linear approximation; 3, the actual thrombin concentration. The level of spatial noise in the reconstructions is 15–25%, the temporal fluctuations of thrombin around its mean are 10–15%, and the error in determining the absolute thrombin concentration is about 10%.

processing uniform signals, but they do not warrant its adequacy in the case of essentially spatially nonuniform distributions. We tested this algorithm for diverse spatial distributions of activated factors in numerical experiments (see Appendix B). Their results suggested that the accuracy of this method for reconstructing the distributions was much better than that of the experimental data.

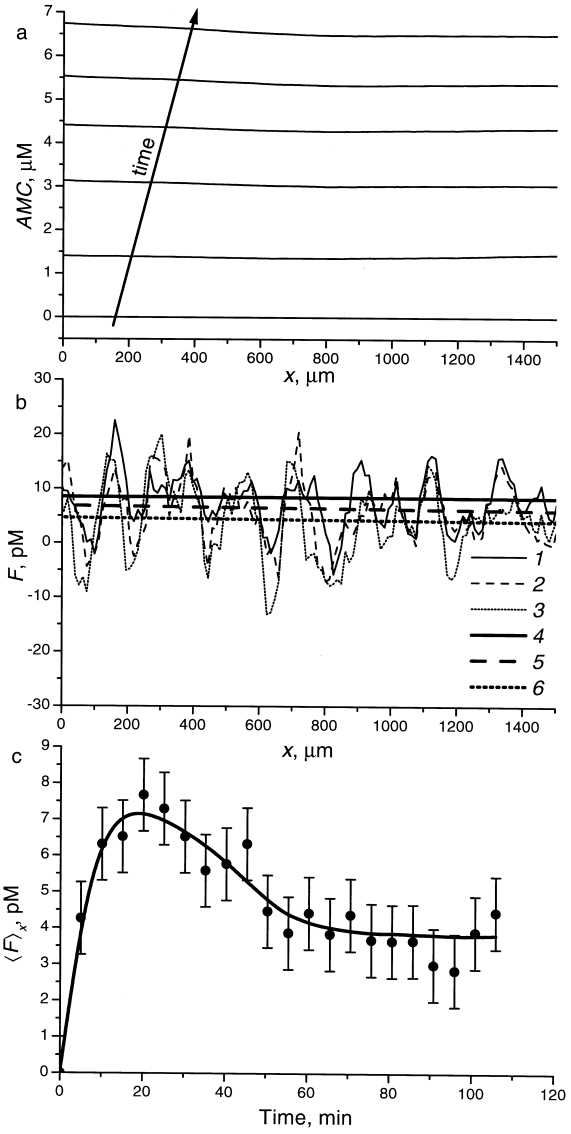

Fig. 5. Algorithm validation in constant source experiments (activation of plasma by a polystyrene surface (dish bottom)). (a) AMC profiles separated by 20 min intervals (from a series recorded at 5 min intervals) in a nonstirred plasma sample (a control sample treated as usually (see Section 2) but without submersing a glass capillary); the first profile was recorded immediately after filling a Petri dish with plasma. The AMC concentration rose uniformly throughout the dish at a low rate. (b) Active factor distributions reconstructed using our algorithm (see Section 2) from the data in panel a for (1) 20, (2) 40, and (3) 100 min from the start of the experiment and their linear approximations (line 4, 5, and 6, respectively). (c) Mean activity determined by averaging the reconstructed active factor distribution over space ($\langle F \rangle_x$) plotted versus time. The concentration of AMC-generating factors did not rise up to more than 7–8 pM, which was three orders of magnitude smaller than those observed in glass-activated plasma (see Fig. 10a).

2.3.5. Deriving the kinetics of clotting factor activation from the AMC distribution

To compare the data of experiments in stirred and nonstirred plasma, the AMC(x,t) distributions were processed to derive the dependence of the total amount of active factors in a sample on time, $F(t)$. Using weight coefficients to take account of radial symmetry of the experiment, we calculated the increase in the total amount of AMC in the sample in a given time period from the AMC(x,t) plots and thereby determined the AMC production rate as a function of time, $V_{AMC}(t)$. As the total amidolytic activity of plasma toward substrate S is described by the Michaelis scheme (see Fig. 9c) and the amount of the substrate hydrolyzed is not large during the first 20–30 min of the experiments (see Fig. 10c), the $V_{AMC}(t)$ thus calculated is proportional to the total amount of activated factors in that sample, $F(t)$. We could monitor $F(t)$ in this way while AMC still remained entirely within the field of view (20–30 min) and its total amount could be determined.

3. Results

3.1. Recording the spatial distribution of activated factors

Under our experimental conditions (Fig. 2), plasma was in contact with a polystyrene Petri dish's bottom (from below), glass tube (activator) walls (at the center of the plasma layer), and a polystyrene plate that was set on the glass tube (from above). The contribution of the polystyrene surfaces was assessed in control experiments in which plasma samples were processed as usually, but no glass tube was submersed into them (Fig. 5). Over 2 h of the experiment (Fig. 5a), the AMC concentration rose uniformly throughout the dish and very slowly, at a rate of about 1 nM AMC/s, which was less than one hundredth of the rate observed at the surface of a glass capillary (see Fig. 6b).

The spatial distribution of amidolytic activity near the activator was quantitatively studied in a thin layer of nonstirred plasma. A 2 ml aliquot of substrate S-containing plasma was poured into a Petri dish, which was transferred to a thermostat to allow the sample to equilibrate at 37°C. After this, a glass capillary was let down into the plasma (Fig. $6a_1$). A total of 15 experiments were performed. The spatial dynamics of AMC concentration changes were qualitatively similar in all experiments. Quantitatively, individual differences were less than 35%. In some 4–5 min, a bright fluorescence ring with clear-cut margins developed around the glass capillary (Fig. $6a_{5,6}$). Thereupon, the ring significantly increased in size, and as it grew up, its boundary became more and more blurred (Fig. $6a_{7-18}$). Eventually (1.5–2 h later), the fluorescence

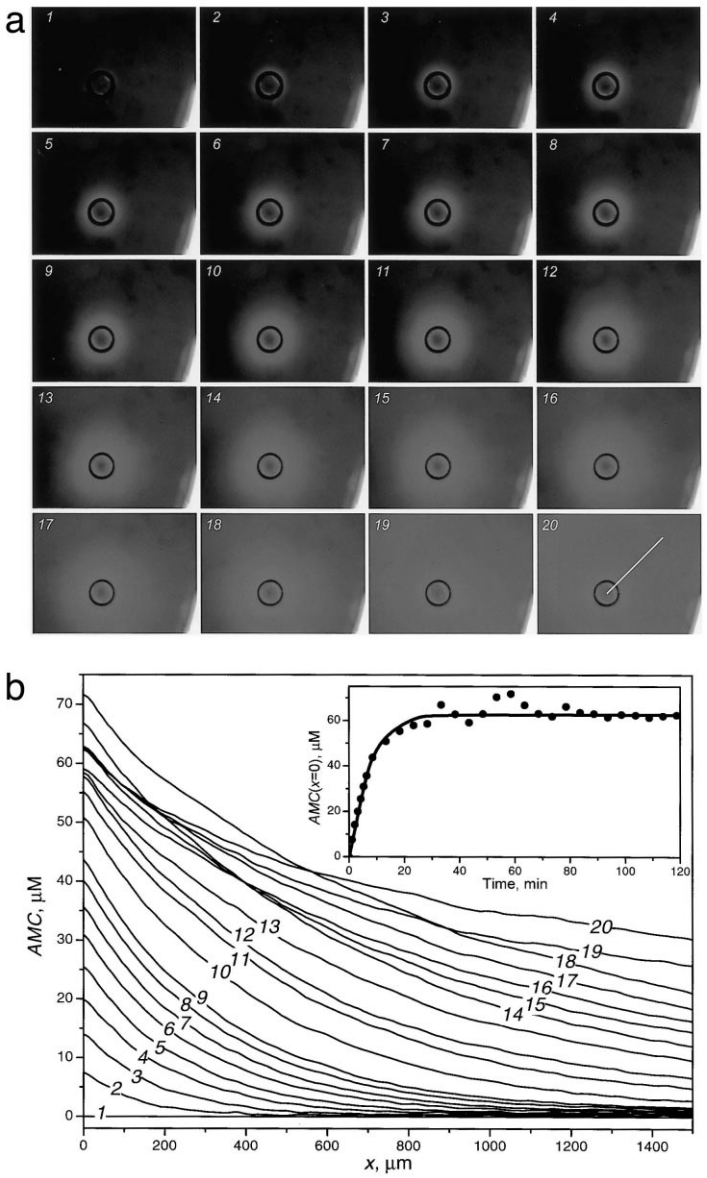

Fig. 6. (a) Time lapse imaging of AMC fluorescence arising in glass-activated plasma (2 ml) supplemented with substrate S (500 μM); a series of 20 frames, with frame 1 taken at the start of the experiments, frames 2–9 at 1 min intervals, 10–17 at 5 min intervals, 18 at a 10 min interval, and 19 and 20 at 30 min intervals (the last frame, 20, was taken 2 h after the start of the experiment). Activator is at the center and the constantly fluorescing label is at the bottom right of every frame; frame dimension is 5.6×7.5 mm. (b) AMC profiles along the scan line indicated in frame 20 for all of the frames shown in panel a. (Inset to panel b) AMC concentration at the glass surface plotted versus time.

was almost uniformly distributed over space (Fig. $6a_{19,20}$). Fig. 6b shows an AMC profile along a scan line depicted in Fig. $6a_{20}$, which was arbitrarily drawn in a radial direction. By design of the experiment, the AMC distribution must possess central symmetry, that is, be independent of the scan line direction. The profiles along different directions did not differ from one another by more than 10% (data not shown). A family of curves in Fig. 6b shows how the spatial AMC distribution varied over time. Throughout the experiment, its maximum was at the activator surface. This shape of the distribution is typical of a diffusion-driven process.

Time series of AMC fluorescence images, like the one presented in Fig. 6a, make it possible to construct a number of kinetic dependences. Shown in the inset to Fig. 6b is the progression curve for AMC production at the glass surface. Obviously, the AMC concentration increased most rapidly over the first 8–10 min, then more and more slowly, leveling off in some 30 min after the start of activation. Yet another dependence derived from the time series of AMC fluorescence images is shown in Fig. 7a (curve 5): the total rate of AMC production by glass-activated plasma in a dish as a function of time. It was possible to construct this plot for the first 30 min of the

experiment while the AMC generated still remained within the field of view of the setup. The rate of AMC production passed through a maximum 10 min after the start of activation, slightly decreased, and then remained constant (Fig. 7a, curve 5). As shown below, only 25% of the substrate was hydrolyzed over this period (Fig. 10c). Therefore, the observed changes in the AMC generation rate (Fig. 7a, curve 5) are likely to reflect the changes in the total amount of activated factors in the sample, rather than to stem from substrate depletion. Analogous information may be obtained in experiments with fully stirred plasma.

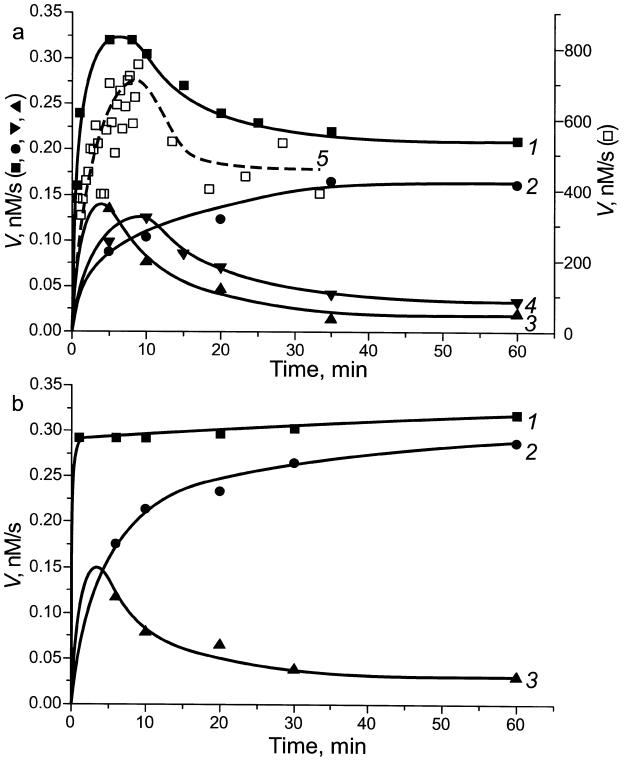

Fig. 7. Kinetics of (a) substrate S and (b) S_k cleavage in glass-activated (1–4) stirred and (5) nonstirred plasma: 1, 5, total activity; 2, activity accounted for by kall–α_2MG complex (residual activity after addition of 200 μg/ml SBTI); 3, kallikrein (the difference between the activity inhibited by 200 μg/ml SBTI and the activity inhibited by 250 μg/ml LBTI); 4, factor XIa (the activity inhibited by 250 μg/ml LBTI; note that only substrate S is cleaved by this factor). See Fig. 1 for the experimental conditions and the reaction mixture composition in stirred plasma. Substrates S and S_k were used at a final concentration of 10 and 25 μM, respectively. The reaction was started by addition of glass beads (100 mg). For determining the contributions of individual factors to the total amidolytic activity, see Section 3.2. In nonstirred plasma (5), the AMC production rate was obtained by pairwise processing of the profiles, that is, by subtracting the area under each antecedent profile from the area under the subsequent profile and dividing the difference by the interval between the frames. The kinetics in nonstirred plasma was monitored for only 30 min, after which AMC diffused beyond the field of view of the setup, making it impossible to quantify its amount by integrating its profile over coordinate.

3.2. Kinetics of factor activation in experiments with full stirring

In glass-activated plasma, the rate at which AMC was cleaved from substrate S varied with time. In all experiments ($n = 10$), its rapid increase during the first 5–10 min was followed by a decrease to 75–90% of the peak value during the subsequent 10–15 min. Thereafter, the rate did not change (Fig. 7a, curve 1). The kinetics of substrate S_k hydrolysis was somewhat different. The rate of AMC accumulation rapidly increased for 1.5–3.0 min and then remained constant for 1 h (Fig. 7b, curve 1). The substrate depletion in these experiments was negligible (10% for substrate S and about 4% for substrate S_k per 1 h). Comparing the kinetics of AMC formation from substrate S in stirred (Fig. 7a, curve 1) and nonstirred (Fig. 7a, curve 5) plasma reveals their close qualitative similarity.

The AMC production rate versus time curve passes through a maximum (Fig. 7a, curve 1), suggesting that the ratio between the substrate S-cleaving factors changed in the course of the reaction. Note that, in studies with purified factors [12] and with plasma [10], factor XIa, kallikrein, and kall–α_2MG complex were found to be active against S_{2366}, which is the same as our substrate S but contains a chromogenic group in place of AMC. Kallikrein and kall–α_2MG complex are known to cleave substrate S_k [14]. To determine the individual contributions of these factors to the overall substrate cleavage in plasma activated by glass, we used two inhibitors, SBTI (200 μg/ml; immediate complete inhibition of factor XIa and kallikrein [12]) and LBTI (250 μg/ml; immediate complete inhibition of factor XIa, but no effect on kallikrein [12]). When constructing the kinetic curves, we performed for each data point the following experiment. Two plasma aliquots containing 10 μM substrate S were stirred for 20 min at 37°C prior to activation (addition of 100 mg of glass beads) and then for time t after activation. At that moment, 200 μg/ml SBTI were added to one aliquot and 250 μg/ml LBTI to the other. For $t < 10$ min, the effect of substrate depletion was negligible: no more than 3% of the substrate was spent by the end of the experiment. For $t \geq 10$ min, substrate was added 7 min prior to the inhibitor. The activity not inhibited by SBTI was some parasitic signal (presumably from the kall–α_2MG complex). As the LBTI-inhibited activity at time t after activation corresponded to the activity of factor XIa, the kallikrein contribution at that moment was the difference between the SBTI- and LBTI-inhibited activities.

The amidolytic activity was completely inhibited by SBTI in α_2MG-deficient plasma (data not shown), but only partially in normal plasma (Fig. 7, curve 2). Hence, it was the kall–α_2MG complex that accounted for the parasitic activity against substrate S. As expected, the rate of AMC production by this complex was initially quite low. It progressively increased for 20–30 min, becoming a major source of AMC-producing activity by

the end of that period. At the concentrations that we used, LBTI inhibited only factor XIa. The fraction of the amidolytic activity of plasma that was inhibited in the presence of LBTI is depicted in Fig. 7a (curve 4). It is likely that this curve reflects the kinetics of substrate S cleavage by factor XIa. The peak of its activity was observed 10 min after addition of glass beads. Only 25% of the peak activity remained 1 h after activation. The use of the two inhibitors made it possible to determine what was the contribution of kallikrein. The difference between the fraction inhibited by SBTI and the fraction inhibited by LBTI is accounted for by the amidolytic activity of kallikrein (Fig. 7, curve 3). Its peak was observed 1–3 min after addition of glass beads, much earlier than the peak activity of factor XIa. In general, kallikrein and factor XIa were generated with similar kinetics.

It was more convenient to study the kinetics of kallikrein formation using substrate S_k (Fig. 7b). In experiments with this substrate against which factor XIa is inactive, addition of LBTI did not affect the AMC accumulation rate. Addition of SBTI significantly slowed down substrate S_k hydrolysis, but this effect rapidly diminished with time (Fig. 7b, curve 2), suggesting kallikrein binding with α_2MG. In our opinion, the inhibitable fraction of the AMC production rate (Fig. 7b, curve 3) is indicative of the kallikrein concentration at any given moment of time. The kinetics of kallikrein formation obtained with substrate S_k was similar to that obtained with substrate S (cf. curves 3 in Fig. 7a,b). The experiments in which the kinetics of factor activation and the effects of inhibitors were studied were performed at least in triplicate. Samples of the same plasma varied in the substrate hydrolysis rate by no more than 20%; interdonor variation was on the order of 40%. These variations did not affect the estimates of the K_m value (see below).

The results shown in Fig. 7 were obtained with low substrate concentrations (about 20 μM). In experiments with high substrate concentrations (200 μM), similar kinetic curves for AMC production over the first 10 min of experiment were obtained (Fig. 8), whether with substrate S (curve 1) or substrate S_k (curve 3). After 10 min of experiment the production of factor XIa and kallikrein shown in Fig. 7 notably declines, whereas in Fig. 8 there are no data for this period of time.

In contact-activated plasma, along with free forms of the active factors, there is their fraction bound to the glass surface. We tried to estimate the ratio between free and surface-bound forms of the active factors in the following way. First, glass beads were added to a sample of plasma, and the kinetics of AMC formation in it was recorded for 10 min. This plasma was then removed as completely as possible, and the cuvette with the beads was filled with fresh plasma containing substrate S (Fig. 8, curve 2). Obviously, it was the bead surface-bound factors from the first sample that determined the initial level of amidolytic activity in the second sample. Thus, the surface-bound

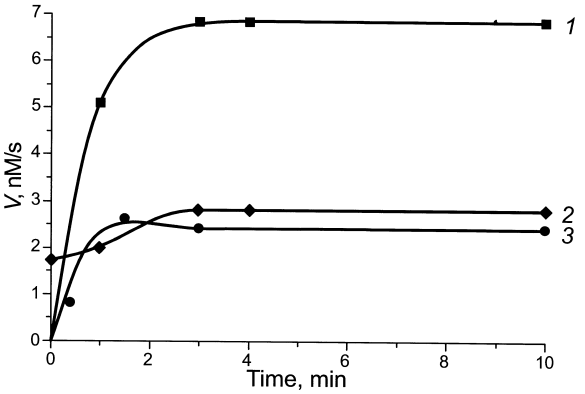

Fig. 8. Kinetics of changes in total amidolytic activity against substrates S (1, 2) and S_k (3) in stirred plasma activated with either (1, 3) 'fresh' glass beads or (2) the glass beads left in the cuvette after curve 1 had been recorded for 10 min (see text for explanation). See Fig. 1 for the experimental conditions and the reaction mixture composition. Substrates S and S_k were used at a final concentration of 200 μM. The reaction was started by addition of glass beads (100 mg); the total glass surface area to plasma volume ratio was 0.12 $mm^2/\mu l$. Note difference in *X*-axis scales between Figs. 7 and 8.

factors accounted for 25% of the activity observed immediately before removing the first plasma sample. In the second plasma sample, the amidolytic activity slightly increased over the first 2 min (Fig. 8, curve 2) and then remained unchanged for 2 h (data not shown).

3.3. Patterns of S and S_k cleavage in plasma

To calculate the spatial distribution of the contact activation factors from the AMC distribution (see Section 2.3.3), we have to know the kinetics of substrate S cleavage. Near a glass capillary's walls in nonstirred plasma, AMC was produced in so great amounts that it would be unjustifiable to neglect substrate depletion any longer. To correctly describe the kinetics of substrate cleavage, we examined how the hydrolysis rate of substrate S or S_k depended on its concentration. The activities of individual contact factors were assessed in these experiments using SBTI and LBTI.

The effect of the substrate concentration on the rate of AMC production 10 min after adding glass beads is shown for substrates S and S_k in Fig. 9a and b (curves 1), respectively. By that time, factor XIa activity in plasma reached its maximum. The same data are presented as Lineweaver–Burk plots in Fig. 9c,d (curves 1). Obviously, for both substrates, the kinetics of their hydrolysis can be approximated by a Michaelis scheme. This analysis yields K_m of 300 μM for substrate S and K_m of 1 mM for substrate S_k. Three enzymes – factor XIa, kallikrein, and kall–α_2MG complex – are known to cleave substrate S. As can be seen in Fig. 7a, they do it at almost equal rates 10 min after the start of activation. Fig. 9a shows how the individual contributions of these enzymes to the overall cleavage rate depended on the substrate concentration (factor XIa, curve 4; kallikrein, curve 3; kall–α_2MG complex,

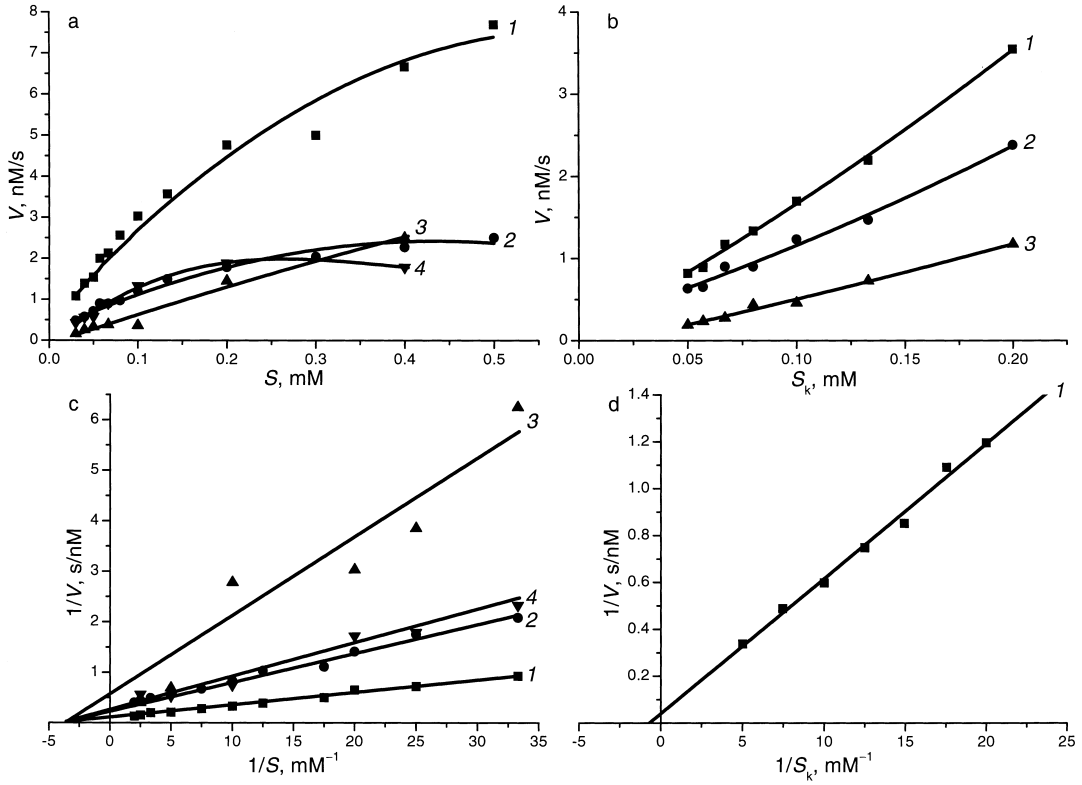

Fig. 9. (a,b) Amidolytic activity (AMC generation rate; V, nM/s) 10 min after addition of glass beads versus substrate concentration and (c,d) Lineweaver–Burk plots for substrates S (a,c) and S_k (b,d): 1, total activity; 2, kall–α_2MG; 3, kallikrein; 4, factor XIa (which cleaves only substrate S). See Fig. 1 for the experimental conditions and the reaction mixture composition. Substrates S and S_k were used at various concentrations. The reaction was started by addition of glass beads (100 mg). See Section 3.2 for the procedure used to determine the contributions of individual factors. For both substrates, the kinetics of their hydrolysis can be approximated well by a Michaelis scheme, with K_m being 300 μM for substrate S and 1 mM for substrate S_k.

curve 2; see Section 3.2 for the experimental procedure). It is easy to demonstrate that the overall rate of substrate cleavage by three enzymes can be described by the Michaelis scheme only if the Michaelis constants of all the enzymes are approximately equal. It was the case for hydrolysis of substrate S, which we used in spatial studies, by factor XIa, kallikrein, and kall–α_2MG complex. Double-reciprocal plots of the data (Fig. 9c, curves 2–4) revealed that these enzymes had similar K_m values of about 300 μM. Note, however, that the accuracy to which this kinetic constant was determined for kallikrein (curve 3) was low. For substrate S_k hydrolysis, the Michaelis constant was determined only roughly, because concentrations as large as tens of millimoles per liter, which were unfeasible in experiments, were required for obtaining more accurate estimates.

Expectedly, these data observed 10 min from the start of activation (addition of glass beads) were similar to those observed at other moments of time (not shown). Therefore, in constructing the program for computing the spatiotemporal dynamics of contact factor activation in nonstirred plasma around a glass capillary, it was natural to assume that only the relationship between the factors changed with time, whereas their Michaelis constants remained the same throughout the experiment.

3.4. Spatial distribution of activated contact factors

Experiments without stirring afford an opportunity of comprehensively addressing the spatiotemporal dynamics of clotting factor activation. Let us first consider the results of experiments in Petri dishes with nonstirred plasma that was not activated by putting down a glass capillary (Fig. 5). Recording the spatiotemporal AMC distributions (Fig. 5a), we calculated (see Section 2.3.3) the spatial distribution of AMC-generating factors (Fig. 5b). As expected, this distribution turned out spatially homogeneous. If we assume that polystyrene and glass activate the same factors, we can construct the plot for the average concentration of activated factors in the dish versus time (Fig. 5c). Their concentration first grew up for 20 min to a maximum of 8 pM or less, then decreased almost by half, and leveled off thereafter.

The results of experiments in which a glass capillary was used to contact activate plasma were processed similarly (Fig. 6). For a series of AMC profiles presented in Fig. 6b, the corresponding activated factor profiles were calculated. Specifically, from the AMC(x,t) recorded, we determined the source function, then the substrate distribution (Fig. 10c), and finally the activated factor distribution and its temporal evolution (Fig. 10a). As can be seen, throughout

the experiment (2 h), the activated factor concentrations are close to zero everywhere but in the narrow zone immediately adjacent to the glass surface (less than 0.1 mm). This result is consistent with the qualitative conclusion that the dependences of the AMC concentration on the time from the start of activation and on the distance from the capillary surface (the AMC(x,t) profiles) are indicative of a diffusion-driven process. This conclusion is prompted by a comparison of the AMC profiles obtained experimentally (Fig. 6b) with those computed under the assumption that the activated factors are bound to the surface and do not diffuse (Appendix B; Fig. 14a). It is as if AMC were generated only at the capillary surface and as if only AMC were capable of diffusing into the bulk, with the activated factors not leaving the surface. Interestingly, similar results were obtained for kininogen in model systems related to the Vroman effect [19]: it was demonstrated that kininogen is fixed and constant at the surface while fibrinogen is removed. The inset to Fig. 10a shows the activated factor distribution in the immediate vicinity of the glass surface obtained using polynomial approximation of the curves in Fig. 10a. Obviously, the concentration is always maximal at the surface, vanishing 80–100 μm away from the surface. This description of the spatial distribution of activated factors in the surface boundary layer is quite rough, because its size is on the order of the spatial resolution of the equipment used. The edge blur width of about 50 μm is comparable with the width of the zone where the concentration of activated factors is likely to be nonzero, that is, about 100 μm. Therefore, we can be confident only that the activated factors (factor XIa and kallikrein) and the 'parasitic' kall–α_2MG complex diffuse no farther away from the glass surface than 0.1 mm.

Fig. 10b shows the factor concentration directly at the glass surface plotted versus time. It rose for 10 min and then leveled off. Only by the end of the 2 h experiment, a slight decrease was observed. This kinetics is in general similar to that obtained for the entire sample (Fig. 7, curve 5). The only distinction is the absence of a decline after the 10th minute.

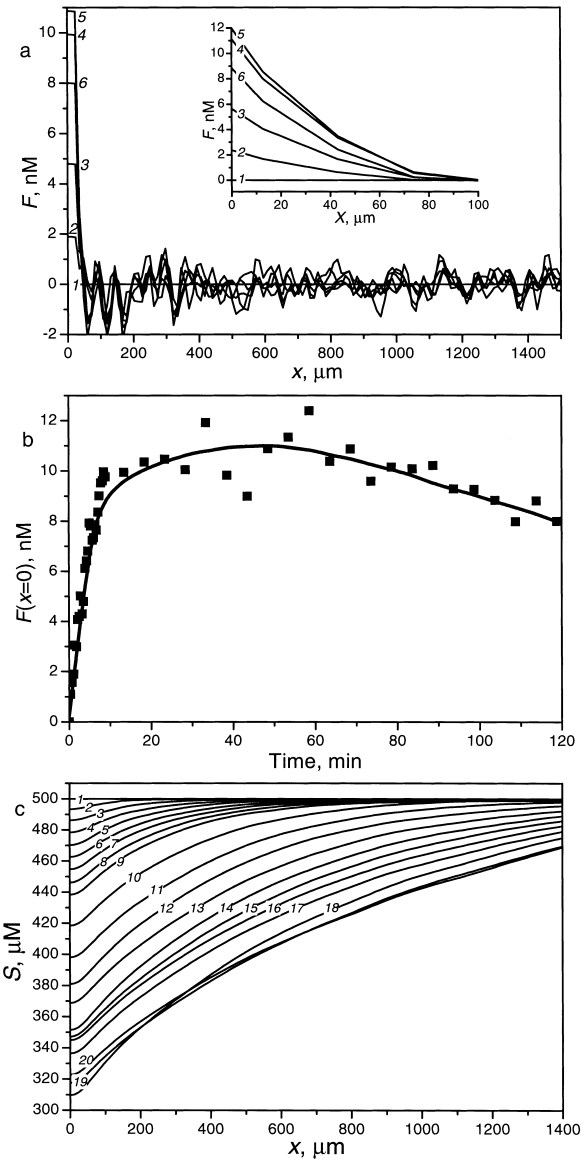

Fig. 10. (a) Activated factor profiles $F(x)$ reconstructed using the proposed algorithm (see Section 2) from the data shown in Fig. 6: (1) at the start of the experiment and at (2) 1, (3) 3, (4) 13, (5) 70, and (6) 120 min thereafter; shown in the inset are the polynomial approximations of these profiles on an expanded scale in the immediate vicinity of the activator. (b) Reconstructed active factor concentration at the glass surface plotted versus time. (c) Reconstructed substrate distributions $S(x)$ (the number at each curve is the same as that of the frame in Fig. 6 to which that curve corresponds).

4. Discussion

In this study, we developed a method for recording the spatiotemporal distributions of activated blood coagulation factors. The method is based on interpreting the images of fluorescence arising from hydrolysis of fluorogenic substrates by these factors. As shown in Section 2, the procedure developed for signal processing eliminates almost all distortions of the fluorescence signal inherent in its recording. The algorithm for interpreting the fluorescence images was tested in numerical experiments, which demonstrated its validity in reconstructing very diverse distributions of active factors (see Figs. 13–15 in Appendix B). Finally, a complete (through) testing of the algorithm was performed in experiments with the known spatial distributions of active factors. The results of fluorescence image processing using this algorithm closely reproduced the distributions that were set experimentally. These experiments also demonstrated that the error in determining the active factor concentrations was greater in the presence of large gradients in the spatial AMC distribution. When processing the data on AMC diffusion (Fig. 3), the pro-

gram correctly inferred that the source function fluctuated around zero, that is, that the dish contained no sources of AMC production. The level of noise in these experiments was up to 100 nM/s. As the substrate with kinetic constants $k_2 = 300\ s^{-1}$ and $K_m = 300\ \mu M$ was usually added to a final concentration of 500 μM in our experiments in nonstirred plasma, the level of 100 nM/s can be easily estimated to be equivalent to the presence of the active factor at a concentration of 500 pM. When a homogeneous thrombin solution was used to produce a signal that was isotropic and did not vary with time (Fig. 4a), the program correctly, to the accuracy of 10%, determined the thrombin concentration (Fig. 4c, curves 2 and 3). In this case, the level of noise across the space was only 30 pM (Fig. 4b, curves 1–3). In experiments in which the activating properties of polystyrene surfaces were studied (Fig. 5), noise was even lower (4–8 pM). Hence, the program developed allows the spatial distributions of active factors to be inferred from the dynamics of fluorescence of a freely diffusing product. This method for studying the dynamics of spatial distributions of activated contact factors can be used to solve the spatial problems with other enzymes, first and foremost, other clotting factors.

4.1. Kinetics of factor activation

The data shown in Figs. 7 and 8 illustrate the activation kinetics of contact factors, kallikrein and factor XIa. Both factors are formed within the first several minutes of activation and then are quite rapidly inactivated via binding with plasma inhibitors. The complex of kallikrein with a plasma inhibitor α_2MG, while being inactive against active clotting factors, retains the capacity to cleave low molecular weight substrates (like those that we used) [14]. Analysis of amidolytic activity of plasma against substrate S using the inhibitors (LBTI and SBTI) demonstrated that its significant fraction during the first 10 min of the experiment was accounted for by factor XIa (30% of the signal; Fig. 7a, curve 4) and kallikrein (25% of the signal; Fig. 7a, curve 3). Thereafter, their contribution to the total amidolytic activity gradually declined, being only 10% for factor XIa and 15% for kallikrein 1 h after the start of activation. Similar data were obtained for kallikrein with substrate S_k (Fig. 7b, curve 3). Thus, contact with glass led to a pulse of generation of active contact factors. Their concentration rose rapidly, reaching a maximum in a few minutes after bringing the plasma in contact with glass, and then gradually decreased because of inactivation by plasma inhibitors. Supposedly, this process is slow because both factor XIa and kallikrein form a complex with high molecular weight kininogen, which protects them against inactivation.

Factor XI and prekallikrein activation is likely to be restricted by the limited number of sites available for binding to the surface. In fact, in experiments with the same glass beads repeatedly used to contact activate two plasma samples, the amidolytic activity rose several times less rapidly and to a lower level in the second (Fig. 8, curve 2) than in the first change of plasma (Fig. 8, curve 1). A plausible explanation of this result is that most of the binding sites on the glass surface are rapidly occupied by contact factors and other plasma proteins during the first incubation with plasma [3,20]; therefore, when the same beads are then incubated with fresh plasma, the number of binding sites for factor XI and prekallikrein on their surface is considerably reduced. These experiments in the homogeneous system (Fig. 8, curve 2) allow us to estimate the fraction of active factors (factor XIa and kallikrein) bound to the surface. As mentioned above (Fig. 7a, curves 3 and 4), both free and surface bound active factors are expected to account for about 50% of the total signal 7–10 min after addition of glass beads. At the time indicated, the total signal in the first sample (Fig. 8, curve 1) was 4 times greater than the initial signal in the second sample (Fig. 8, curve 2); therefore, we concluded that approximately half of the active factors were bound to the glass surface. Supposedly, the surface-bound fraction consisted mostly of factor XIa [5].

In experiments with (polystyrene cuvettes) and without stirring (Petri dishes), the amidolytic activity of glass-activated plasma changed with similar kinetics (Fig. 7a, curves 1 and 5). The rate of substrate S hydrolysis rose rapidly over 5–10 min after the start of activation and then remained almost constant for 1 h. It is of interest to quantitatively compare the amidolytic activity of stirred and nonstirred contact-activated plasma. Stirring makes the

Table 1
Comparison of amidolytic activity of plasma in different experiments

Activator:	Polystyrene		Glass		
Experimental system:	Stirred plasma (Fig. 1)	Nonstirred plasma (Fig. 5)	Stirred plasma (Fig. 7a)	Nonstirred plasma (Fig. 10)	Flow reactor [7]
V_{AMC} (mol/(mm^3 s)$\times 10^{-4}$)	1.5	16	3	150	–
S (mol/mm^3)	10	500	10	500	–
Volume (mm^3)	1800	74	1800	44	36
F_{total} (mol$\times 10^{-16}$)	280	7.4	560	35	720
Area (mm^2)	800	74	220	8.2	240
Surface-bound activity (mol/mm$^2\times 10^{-17}$)	3.5	1	25	43	30

system uniform throughout the sample volume; therefore, the total activity of factors in plasma is easy to assay at any moment of time. In experiments without stirring, the amount of AMC produced can also be determined, which makes it possible to estimate the total activity of factors. The data collated in the first four columns of Table 1 correspond to the moment of 10 min from the start of activation. Knowing the overall rate of AMC production in a cuvette or a Petri dish (V_{AMC} in Table 1) and the substrate S concentration (S) allows the total amount of the active factor (F_{total}) at a given moment to be calculated from the Michaelis relationship:

$$\frac{V_{AMC}}{\text{volume}} = \frac{k_2 S}{K_m + S} F_{total}$$

The F_{total} in Table 1 was calculated assuming that $k_2 = 300\ s^{-1}$, $K_m = 300\ \mu M$. Knowing F_{total} and the area of the activating surface in contact with plasma, one can determine the specific surface-bound activity. Shown in Table 1 is the specific surface-bound activity calculated assuming that the entire factor activity is bound to the surface. In fact, only its fraction is surface-bound. For example, in experiments with glass beads, we estimated this fraction at 50%. However, we could not know how large this fraction was in other variants of experimental design. Therefore, we chose to compare the activities elicited by contact with glass or polystyrene relating them entirely to the activating surface. In this way, we compared the results obtained in stirred plasma with those in nonstirred plasma and the results reported in [7], which were obtained in a capillary flow reactor. In the last case (last column of Table 1), the estimates are rough, and they are given only by way of illustration, because the experimental conditions were not directly comparable: factor XIa was assayed in the flow from the glass capillary outlet. We found that, irrespective of the experimental design, the active factor concentration on the glass surface was $(25–45)\times10^{-17}$ mol/mm^2, which corresponds to about 2×10^8 molecules of the factor per mm^2. This number is only 100–1000 times lower than the limiting one, that is, the number of molecules required for confluent coating of 1 mm^2. The activity bound with the polystyrene surface was found to be 10–40 times lower. The fact that similar estimates were obtained in various experiments with activation of plasma by glass suggests that the presence or absence of stirring only slightly, if any, affects the activating properties of surfaces.

4.2. Spatial distribution of active factors

Experiments in nonstirred plasma provided evidence that active factors diffused no more than 80–100 μm away from the glass surface in 2 h (Fig. 10). It is likely that active factors, that is, factor XIa and kallikrein, reside directly at the glass surface, forming complexes with HMWK, in which they are protected against inhibition.

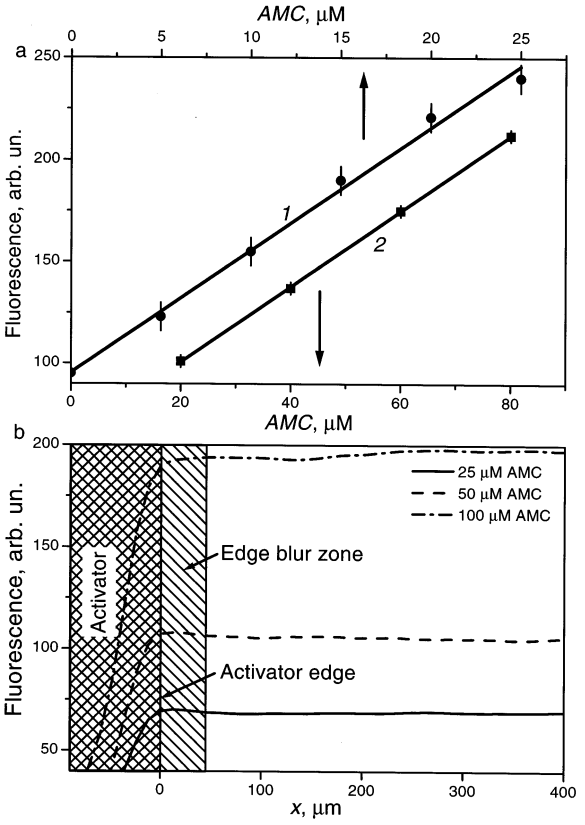

Fig. 11. Setup operation testing: (a) linearity with respect to AMC and (b) signal distortion at the activator surface (edge blur). (a) Fluorescence intensity versus the AMC concentration in the sample. A Petri dish was filled with a buffer containing AMC at different concentrations, and the signal was recorded at the desired sensitivity of the setup. A high sensitivity (as that at which set 1 was recorded) is achieved with long exposure times and wide apertures, making it possible to detect AMC at concentrations comparable with noise, which was equivalent to about 1 μM AMC in our setup. At smaller apertures and shorter exposure times, the sensitivity is lower, and larger signals can be determined (set 2). Thus, the AMC concentrations detectable with this setup range from several micromoles to at least 80 μM. Linear regression of data sets 1 and 2 shows that the fluorescence recorded is proportional to the AMC concentration in the sample (i.e. that the setup is linear with AMC). (b) Fluorescence intensity profiles along a radius drawn out of the center of the activator obtained at different AMC concentrations in the Petri dish. In a region adjacent to the activator surface, the signal is distorted because of insufficiently sharp focusing.

As demonstrated in [5,6], most of the functional factor XIa is bound to the surface. The data reported in [7] also provide indirect evidence that factor XIa activity is mostly surface-bound. A large fraction of kallikrein was found in the bulk [5]; however, those data gave no indication of whether it remained free, retaining its activity, or was inactivated by plasma inhibitors. Consistent with data of others [21], our results suggest that the latter is more likely. One of the inhibitors of kallikrein is α_2MG [21]. Its complex with kallikrein remains active against low molecular weight substrates [14]. The kall–α_2MG complex accounts for the major (75%) fraction of the AMC-produc-

ing activity by the 35th minute from the start of activation (Fig. 7a). It is natural to expect that this complex would be in solution, capable of freely diffusing away from the glass surface into the bulk of plasma [22]. To assess the characteristic diffusion times for this complex, we used a qualitative model wherein the substance that was assumed to freely diffuse into the bulk was kept at a constant concentration at the surface. If its molecular mass were equal to that of the kall–α_2MG complex, that is, 830 kDa [3], it would spread over 0.3 mm in 2 h. To run no more than 0.1 mm in 2 h, it should be about 3000 kDa. Interestingly, contact factors were in fact reported to occur as multimeric complexes [9].

Summing up all aforesaid, we can conclude that the contact factors are mostly restricted to the surface. Supposedly, they are either bound to the surface or form multimeric complexes with inhibitors, which diffuse into the bulk. Factor XIa and free kallikrein spread over distances that were shorter than those expected based on their diffusion characteristics. Let us compare the distances run by these factors with the size of clots formed under similar conditions around glass beads [2]. The clots grew up to 0.5–0.6 mm in 30–40 min. Obviously, their growth could not be fed by factor XIa generated at the glass surface, because, in the time indicated, it would have run no more than 20% of that distance. Therefore, we come to conclude that the main role in clot formation at distances longer than 0.1 mm is played by factor XIa that thrombin generates from factor XI [23,24] in the bulk, rather than by factor XIa formed in the reactions of contact activation at the activating surface.

Acknowledgements

We are grateful to Drs. E.I. Sinauridze, R.I. Volkova, V.I. Zarnitsina and M.V. Ovanesov for fruitful discussions. This study was supported in part by the Russian Foundation for Basic Research (Project 00-04-48855).

Appendix A. Setup operation testing and error elimination

To ensure that fluorescence recordings are free of artifacts, we tested the setup to assess (i) the range of linearity with respect to the AMC concentration; (ii) convection-related effects in plasma; (iii) correctness of image recordings by the camera; (iv) spatial variation of illumination; (v) temporal fluctuations of illumination; and (vi) distortions in fluorescence images. The setup proved to be linear with AMC up to 80 μM, judging from the plots of the fluorescence signal (in arbitrary units) versus the AMC concentration in the sample (Fig. 11a). Observing the Brownian motion of Indian ink or dust particles, we could detect no convective flows (data not shown). The image proportions were somewhat distorted by the camera because of the rectangular shape of its pixels (one side being 1.16 times longer than the other). Illumination was nonuniform across the Petri dish area. This spatial nonuniformity was up to 40% and did not vary with time, unlike the total emitting power of the lamp. The signal was somewhat distorted near the activator surface because of the edge blur (Fig. 11b).

As evident from this analysis, no correction was needed

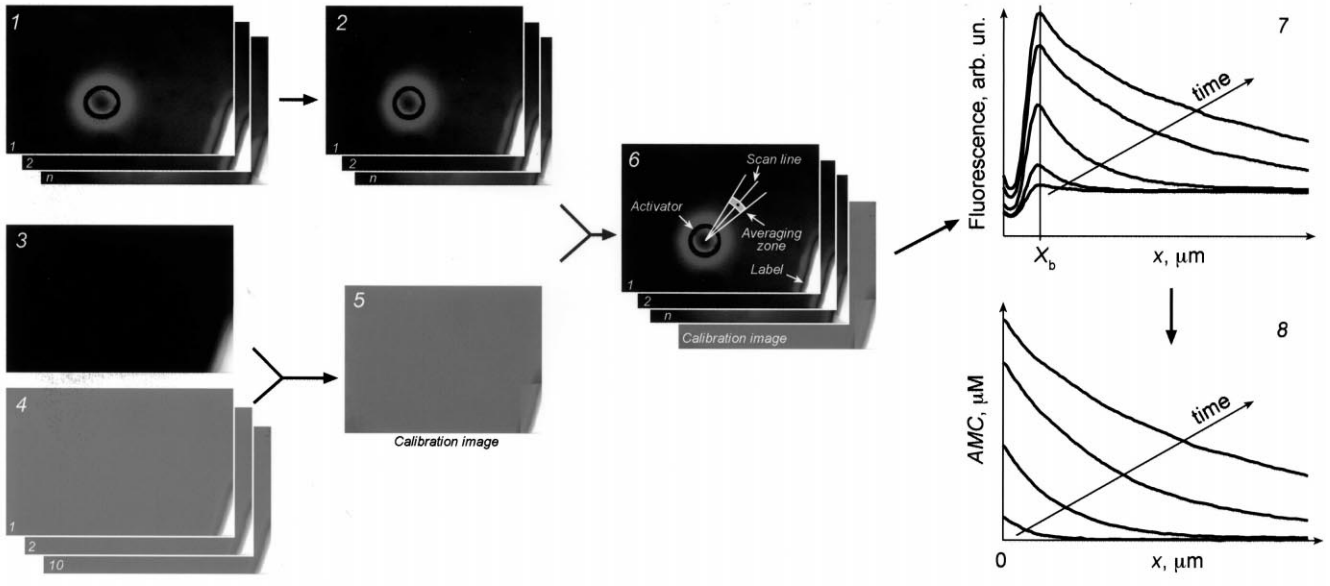

Fig. 12. Scheme of the algorithm for fluorescence image processing: (1) raw images; (2) images with the proportions corrected; (3) background image for calibration; (4) images obtained with the known AMC concentrations (calibration frames); (5) calibration image; (6) complete set of images, drawing a scan line; (7) plots of fluorescence intensity versus distance to the activator center for different moments of time (X_b corresponds to the activator boundary); (8) plots of AMC concentration versus distance to the activator surface for different moments of time.

for AMC nonlinearity or convection-related effects. Most of the drawbacks identified (iii–v) were eliminated using the program for data processing that was developed to reconstruct the actual AMC distribution in the sample.

(iii) To restore the actual proportions, all experimentally obtained images (Fig. 12_1) were 1.16 times compressed along the long axis (Fig. 12_2).

(iv) To determine the AMC concentration from nonuniformly illuminated images, we constructed the calibration image. First, a background frame was taken, that is, an image of a dish with plasma containing no substrate (Fig. 12_3). Second, AMC was added to a known final concentration to a sample of the same plasma, and its image was recorded 10 times (Fig. 12_4). The fluorescence intensity was averaged pixel by pixel over these 10 frames. The average image thus obtained was free of the effect of temporal fluctuations of illumination. The background image was then subtracted from the average image. To smoothen the image, minor imperfections were eliminated using the moving window technique (11×11 pixels), and the image was 1.16 times compressed along the long axis. The resulting calibration image (Fig. 12_5) contained information about the nonuniformity in illumination of the area to be studied and made it possible to calibrate the fluorescence signals recorded in the subsequent frames of the experiment in terms of AMC concentration (Fig. 12_6).

The image was analyzed along an arbitrarily chosen radially directed scan line from the activator center. Using a blue component of the signal, we could go over to a set of one-dimensional profiles of the AMC fluorescence intensity along this scan line for all frames of the experiment, including the calibrating image (Fig. 12_7). To improve the signal-to-noise ratio, the profiles were averaged over a 30° sector adjacent to the chosen scan line. Specifically, the scan line (a median of the sector) was divided into 10 μm intervals. The fluorescence intensity at each division point was defined to be a mean over the area confined by the rays forming the sector and two circular segments drawn through the scan line points lying 15 μm up and down of that point (Fig. 12_6). After this, we marked the point on the scan line corresponding to the activator boundary (X_b). To the right of X_b, we had a set of one-dimensional fluorescence profiles (fluorescence intensity versus distance from the activator).

(v) The effects of temporal fluctuations in illumination (lamp instability) were reduced using the following procedure. The fluorescence intensity of the label (Figs. 2_{12} and 12_6) was measured in every frame, and its mean over all frames was then calculated. When processing fluorescence signals in a frame, we normalized them to the ratio of the signal from the label in that frame to its signal averaged over all frames in that experiment.

The first frame in the experiment was taken immediately after submersing the activator into the sample; while still free of the useful signal, it served as the background component subtracted from all the subsequent frames during processing the signals along the chosen scan line. The next step in the processing was to divide out the effects of the spatial nonuniformity of illumination and to calibrate the signals in AMC concentration units, which was done by normalizing the signal to the calibration image. In this way, we reconstructed the actual AMC distribution along the chosen scan line, that is, AMC(x,t) describing the AMC concentration as a function of the distance from the activator and the time from the start of activation (Fig. 12_8). After implementing this procedure, the error associated with the spatial nonuniformity of illumination was no more than 5% and that associated with the temporal lamp instability no more than 15%.

(vi) The only drawback that defied attempts to eliminate it was the distorted AMC distribution in the narrow layer adjacent to the plasma–activator interface (Fig. 11b). The source of this limitation was the apertures used, which were insufficiently low with the 2 mm thick plasma layer to have the depth of field that would allow sharp focusing. For this reason, regions with large signal gradients (as those in contact with the activator surface) were substantially smoothed in the image. The width of the smoothed zone, which depended on the boundary gradient of AMC, was 30–50 μm in our experiments. Therefore, we could determine AMC(x,t) significantly everywhere except in this zone.

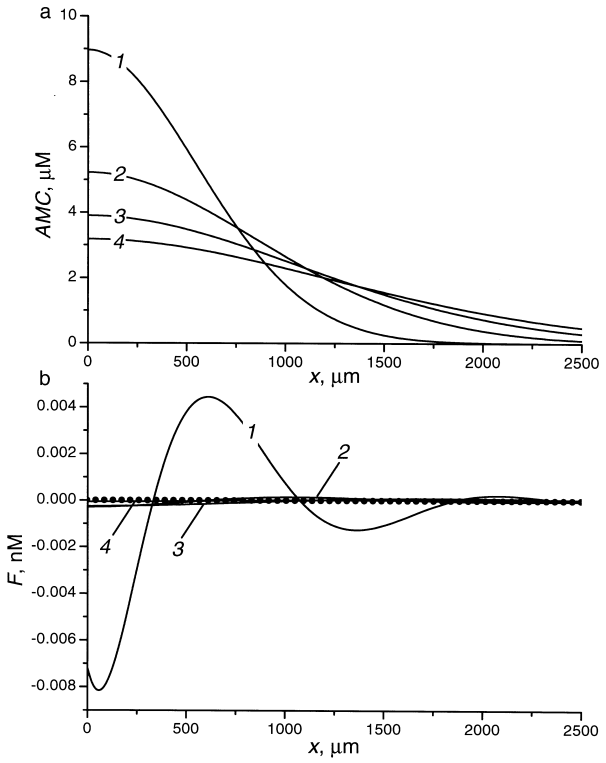

Fig. 13. Numerical testing experiment with the zero signal: $F(x,t) = 0$ (panel b, dots). The initial AMC distribution was set in the form $AMC_0 = 100$ μM for $0 < X < 30$ μm and $AMC_0 = 0$ μM for $X > 30$ μm (not shown). (a) Diffusion-related redistribution of AMC simulated in the model. (b) $F(x,t)$ (lines) reconstructed using the algorithm developed from the data shown in panel a for (1) 4, (2) 10, (3) 16, (4) 22 min after the start of the experiment (selected from a series of reconstructed curves at 2 min intervals).

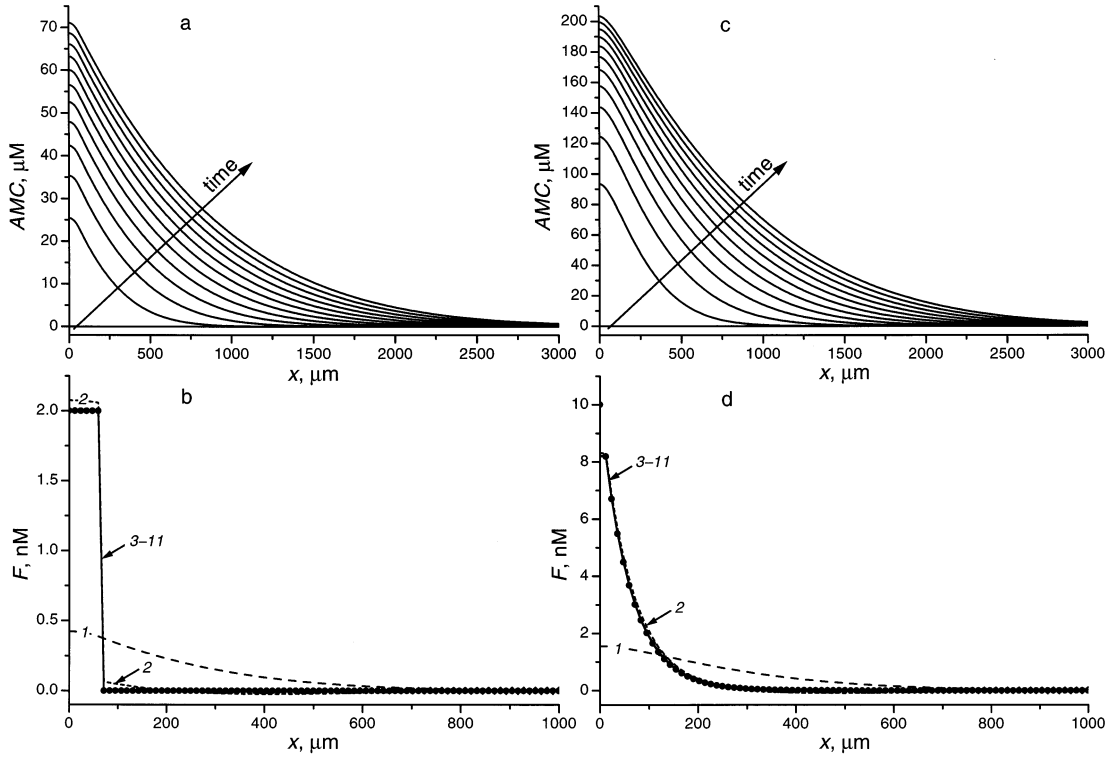

Fig. 14. Numerical testing experiments with signals (dots) that do not vary with time: $F(x,t) = F_0(x)$, where $F_0(x)$ is either a step (b) or a descending exponential function of coordinate (d). (a,c) AMC(x,t) distributions simulated in the model for signals (dots) shown in panel b and d, respectively; the interval between the curves is 2 min. (b,d) Lines, active factor distributions $F(x,t)$ reconstructed from the AMC(x,t) distributions shown in panel a and c, respectively. The first reconstructed profile corresponds to 2 min after the start of the experiment; others follow at 2 min intervals (curves 3–11 coincide). The reconstructed distributions (lines) coincide with the initially set distributions (dots) at the third and all the subsequent time steps. Note difference in X-axis scales between panels a, c and b, d.

Appendix B. Numerical testing experiments

As shown above, the main steps in calculation of the spatial distribution of active factors in the sample are the elimination of errors in fluorescence recordings and the interpretation of the corrected data with allowances for AMC diffusion and substrate depletion. The interpretation algorithm was validated in numerical experiments using the mathematical model of contact activation described elsewhere [25,26]. We set some spatial distribution of active factors $F(x,t)$ and computed the AMC(x,t) generated in the model by this distribution and diffusion. After this, we discretized the simulated AMC(x,t) in space and time with steps characteristic of our experiments ($dx = 10$ μm, $dt = 2$ min) and tried to reconstruct the initially set $F(x,t)$ using the algorithm described above. In these simulations, the $F(x,t)$ distributions were varied broadly to span all situations likely in experiments.

'Zero' signal

If plasma contains no active factors, $F(x,t) = 0$ (Fig. 13b, dots). The initial AMC distribution was set as follows: $AMC_0 = 100$ μM for $0 < X < 30$ μm and $AMC_0 = 0$ μM for $X > 30$ μm (data not shown). Using the model, we calculated the diffusion-related redistribution of AMC (Fig. 13a). These data were then used to reconstruct $F(x,t)$ (Fig. 13b, lines) with our algorithm. As can be seen, the reconstructed $F(x,t)$ (in effect, the error of interpretation in this case) exponentially tends to zero with time, indicating that the algorithm performs well in the absence of the signal.

Signal not varying with time

The active factor distribution in plasma was set independent of time $F(x,t) = F_0(x)$ either as a step (Fig. 14b, dots) or a descending exponential (Fig. 14d, dots) function of coordinate, and the corresponding AMC(x,t) distributions (lines in Fig. 14a and c, respectively) were simulated using the model. Thereafter, the simulated data were used to reconstruct the active factor distributions (Fig. 14b,d, lines). The profiles reconstructed for the first time point (lines 1 in Fig. 14b,d) differed considerably from those set initially. This result is expected because it is always assumed in the program that no active factors exist at time zero, according to our experimental protocol. However, the algorithm rapidly converges, and the set and the reconstructed profiles become similar as early as at the second time step (lines 2 in Fig. 14b,d) and fully coincident at the third time step and thereafter (lines 3–11 in Fig. 14b,d).

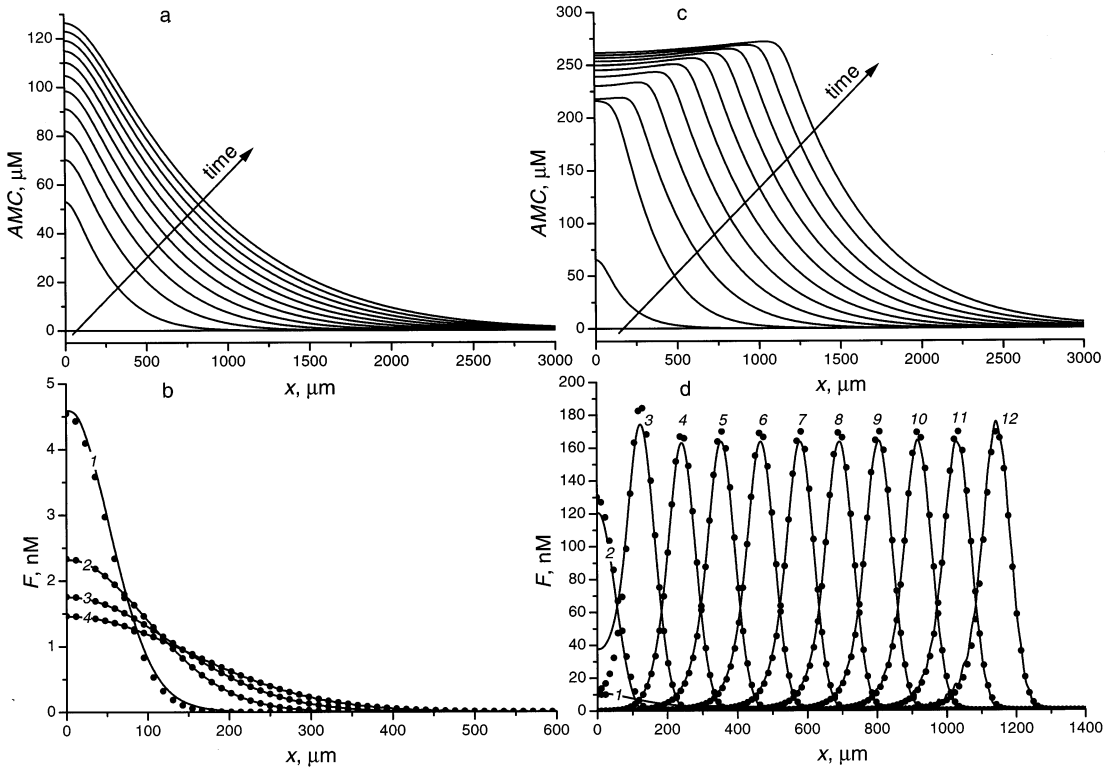

Fig. 15. Numerical testing experiments with signals varying over time and space: $F(x,t) = F_i(x)$, where $F_i(x)$ is either an exponential function that varies with time remaining self-similar (b, dots), or a running autowave of constant amplitude (d, dots). (a,c) AMC(x,t) distributions simulated in the model for signals shown in panel b and d (dots), respectively; the interval between the curves is 2 min. (b,d) Lines, active factor distributions $F(x,t)$ reconstructed from AMC(x,t) shown in panel a and c, respectively. The first reconstructed profile corresponds to 2 min after the start of the experiment; others follow at 2 min intervals. In panel b, shown are the first four out of 12 profiles simulated at 2 min intervals. The reconstructed distributions (lines) coincide with the initially set distributions (dots) as early as at the first time step. Note difference in X-axis scales between panels a, c and b, d.

Signal varying over time and space

The active factor distribution in plasma was set in the form $F(x,t) = F_i(x,t)$, where $F_i(x,t)$ is either an exponential function that varies with time remaining self-similar (Fig. 15b, dots), or a running autowave of constant amplitude (Fig. 15d, dots). Their reconstructions (Fig. 15b,d, lines) from the respective AMC(x,t) distributions simulated in the model (Fig. 15a,c) were almost identical to the originally set functions.

Hence, the algorithm proposed for deriving the $F(x,t)$ from the AMC distributions performs well in all the cases of $F(x,t)$ considered, which span the entire range of situations that are possible in experiments.

References

[1] J. Jesty, Y. Nemerson, The pathways of blood coagulation, in: E. Beutler, M.A. Lichtman, B.S. Coller, T.J. Kipps (Eds.), Williams Hematology, 5th edn., McGraw-Hill Health Professions Division, New York, 1995, pp. 1227–1239.

[2] F.I. Ataullakhanov, G.T. Guria, V.I. Sarbash, R.I. Volkova, Spatio-temporal dynamics of clotting and pattern formation in human blood, Biochim. Biophys. Acta 1425 (1998) 453–468.

[3] J.C.M. Meijers, B.A. McMullen, B.N. Bouma, The contact activation proteins: a structure/function overview, Agents Actions 38 (Suppl.) (1992) 219–230.

[4] F. Espana, O.D. Ratnoff, The role of prekallikrein and high-molecular-weight kininogen in the contact activation of Hageman factor (factor XII) by sulfatides and other agents, J. Lab. Clin. Med. 102 (1983) 487–499.

[5] R.C. Wiggins, B.N. Bouma, C.G. Cochrane, J.H. Griffin, Role of high-molecular-weight kininogen in surface-binding and activation of coagulation factor XI and prekallikrein, Proc. Natl. Acad. Sci. USA 74 (1977) 4636–4640.

[6] S.D. Revak, C.G. Cochrane, B.N. Bouma, J.H. Griffin, Surface and fluid phase activities of two forms of activated Hageman factor produced during contact activation of plasma, J. Exp. Med. 147 (1978) 719–729.

[7] R. Blezer, G.M. Willems, P.T. Cahalan, T. Lindhout, Initiation and propagation of blood coagulation at artificial surfaces studied in a capillary flow reactor, Thromb. Haemost. 79 (1998) 296–301.

[8] R.W. Colman, L. Matter, S. Sherry, Studies on the prekallikrein-kallikrein enzyme system of human plasma, J. Clin. Invest. 48 (1969) 11–32.

[9] N.O. Hoem, S. Johannesen, K. Briseid, Formation of an association between factor XII and kallikrein in human plasma – significance of storage of plasma and the functional state of plasma kallikrein, Thromb. Res. 66 (1992) 421–434.

[10] K. Briseid, N.O. Hoem, S. Johannesen, K. Haug, Amidolytic assay of factor XI in human plasma – significance of kallikrein for the activity measured, Thromb. Res. 78 (1995) 239–250.

[11] M. Schapira, C.F. Scott, R.W. Colman, Contribution of plasma pro-

tease inhibitors to the inactivation of kallikrein in plasma, J. Clin. Invest. 69 (1982) 462–468.
[12] G. Tans, T. Janssen-Claessen, J. Rosing, J.H. Griffin, Studies on the effect of serine protease inhibitors on activated contact factors, Eur. J. Biochem. 164 (1987) 637–642.
[13] S. Kawabata, T. Miura, T. Morita, H. Kato, K. Fujikawa, S. Iwanaga, K. Takada, T. Kimura, S. Sakakibara, Highly sensitive peptide-4-methylcoumaryl-7-amide substrates for blood-clotting proteases and trypsin, Eur. J. Biochem. 172 (1988) 17–25.
[14] M.J. Gallimore, Chromogenic peptide substrate assays for determining components of the plasma kallikrein system, Scand. J. Clin. Lab. Invest. 45 (1985) 127–132.
[15] E.I. Sinauridze, R.I. Volkova, Y.V. Krasotkina, V.I. Sarbash, F.I. Ataullakhanov, Dynamics of clot growth induced by thrombin diffusing into non-stirred citrate human plasma, Biochim. Biophys. Acta 1425 (1998) 607–616.
[16] N.N. Kalitkin, Numerical Methods (in Russian), Nauka, Moscow, 1978, pp. 132–135.
[17] A.N. Tihonov, A.A. Samarskii, Equations of Mathematical Physics (in Russian), Nauka, Moscow, 1966, pp. 228–230.
[18] A.G. Marshal, Biological Chemistry: Principles, Technics, and Applications, John Wiley and Sons, New York, 1978, p. 159.
[19] M.T. Le, P. Dejardin, Simultaneous adsorption of fibrinogen and kininogen at a silica/solution interface, Langmuir 14 (1998) 3356–3364.
[20] R.C. Eberhart, M.S. Munro, J.R. Frautschi, M. Lubin, F.J. Clubb Jr., C.W. Miller, V.I. Selivanov, Influence of endogenous albumin binding on blood-material interactions, Ann. NY Acad. Sci. 516 (1987) 78–95.
[21] F. Graaf, J.A. Koedam, B.N. Bouma, Inactivation of kallikrein in human plasma, J. Clin. Invest. 71 (1983) 149–158.
[22] C.F. Scott, A. James, L.D. Silver, F. Kueppers, H.L. James, R.W. Colman, High molecular weight kininogen or its light chain protects human plasma kallikrein from inactivation by plasma protease inhibitors, Biochemistry 21 (1982) 567–572.
[23] D. Gailani, G.J. Broze Jr., Factor XII-independent activation of factor XI in plasma effects of sulfatides on tissue factor-induced coagulation, Blood 82 (1993) 813–819.
[24] P.A. von dem Borne, J.C. Meijers, B.N. Bouma, Feedback activation of factor XI by thrombin in plasma results in additional formation of thrombin that protects fibrin clots from fibrinolysis, Blood 86 (1995) 3035–3042.
[25] V.I. Zarnitsina, A.V. Pokhilko, F.I. Ataullakhanov, A mathematical model for the spatio-temporal dynamics of intrinsic pathway of blood coagulation. I. The model description, Thromb. Res. 84 (1996) 225–236.
[26] V.I. Zarnitsina, A.V. Pokhilko, F.I. Ataullakhanov, A mathematical model for the spatio-temporal dynamics of intrinsic pathway of blood coagulation. II. Results, Thromb. Res. 84 (1996) 333–344.